



Highly Fluorescent Magnetic Nanobeads with a Remarkable Stokes Shift as Labels for Enhanced Detection in Immunoassays

Francesca Salis, Ana B. Descalzo,* Elena Benito-Peña, María C. Moreno-Bondi, and Guillermo Orellana*

Fluorescence immunoassays are popular for achieving high sensitivity, but they display limitations in biological samples due to strong absorption of light, background fluorescence from matrix components, or light scattering by the biomacromolecules. A powerful strategy to overcome these problems is introduced here by using fluorescent magnetic nanobeads doped with two boron-dipyrromethane dyes displaying intense emission in the visible and near-infrared regions, respectively. Careful matching of the emission and absorption features of the dopants leads to a virtual Stokes shift larger than 150 nm achieved by an intraparticle Förster resonance energy transfer (FRET) process between the donor and the acceptor dyes. Additionally, the magnetic properties of the fluorescent beads allow preconcentration of the sample. To illustrate the usefulness of this approach to increase the sensitivity of fluorescence immunoassays, the novel nanoparticles are employed as labels for quantification of the widely used Tacrolimus (FK506) immunosuppressive drug. The FRET-based competitive inhibition immunoassay yields a limit of detection (LOD) of 0.08 ng mL⁻¹, with a dynamic range (DR) of 0.15–2.0 ng mL⁻¹, compared to a LOD of 2.7 ng mL⁻¹ and a DR between 4.1 and 130 ng mL⁻¹ for the immunoassay carried out with direct excitation of the acceptor dye.

excitation light.^[1] To overcome these problems, different strategies are described in the literature including: i) to take advantage of very brilliant tags (i.e., highly fluorescent tracers with large absorption coefficients) to achieve a strong analytical signal; ii) detection in the near-infrared (NIR) region of the spectrum to minimize autofluorescence from the sample;^[2] iii) intensification of the analytical signal by simultaneous labeling with fluorophore ensembles;^[3] iv) to set the largest possible separation between the excitation and emission wavelengths for avoiding interference from the light scattering, and v) sample preconcentration to decrease the limit of detection (LOD). All the strategies mentioned above are even more relevant when aiming to determine directly the concentration of disease markers or drugs in serum or blood.^[4]

The current standard technique in clinical chemistry to analyze the concentration of chemicals in blood is liquid chromatog-

1. Introduction

Sensitive optical detection in biological samples is a demanding task due to common features of biological matrices namely, the presence of colored species (e.g., hemoglobin), fluorescent components (such as tryptophan, tyrosine, or phenylalanine amino acids, vitamins, etc), and particles that scatter the

raphy/mass spectrometry (LC/MS) or liquid chromatography/mass spectrometry-mass spectrometry (LC/MS-MS).^[5] However, the associated methods are laborious, expensive, bulky, and do not allow even an in situ semicontinuous monitoring of the analyte levels (e.g., for point-of-care-testing or POCT). Immunoassays are alternative analytical methods for sensitive and selective determination of the target, particularly when combined with fluorescence detection of the analyte or, more often, of a fluorescent-labeled drug or antibody.^[4] Nevertheless, the strong absorption of light and the background fluorescence from other matrix components, or the light scattering by the biomacromolecules, frequently decrease the immunoassay performance.

Immunosuppressive drugs have become a fundamental pillar in the success of organ transplantation.^[5] In this regard, a particularly relevant drug is Tacrolimus (also coded FK506 by the original manufacturer, Scheme S1 in the Supporting Information), a hydrophobic 23-membered macrolide lactone produced by *Streptomyces tsukubaensis*,^[6] the powerful immunosuppressive effect of which relies on the disruption of signaling events mediated by calcineurin in T lymphocytes.^[7] FK506 and other immunosuppressants require frequent monitoring

F. Salis, Prof. A. B. Descalzo, Prof. G. Orellana

Department of Organic Chemistry

Faculty of Chemistry

Complutense University of Madrid (UCM)

28040 Madrid, Spain

E-mail: ab.descalzo@quim.ucm.es; orellana@quim.ucm.es

Prof. E. Benito-Peña, Prof. M. C. Moreno-Bondi

Department of Analytical Chemistry

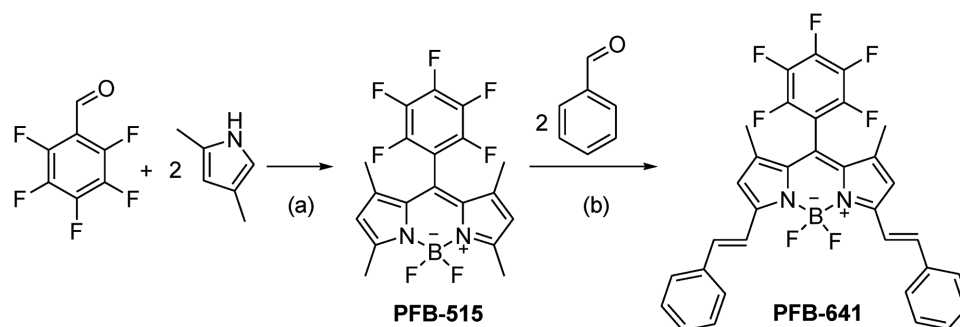
Faculty of Chemistry

Complutense University of Madrid (UCM)

28040 Madrid, Spain

The ORCID identification number(s) for the author(s) of this article can be found under <https://doi.org/10.1002/sml.201703810>.

DOI: 10.1002/sml.201703810



Scheme 1. Synthesis of a) PFB-515 and b) PFB-641. a) (i) TFA, CH_2Cl_2 , Ar, rt; (ii) chloranil, CH_2Cl_2 , rt; (iii) $\text{BF}_3 \cdot \text{Et}_2\text{O}$, Et_3N , CH_2Cl_2 , rt, and, b) piperidine, toluene, reflux.

in transplanted patients because of the inter- and intrasubject variability of the pharmacokinetics, and the diverse correlation between the administered dose and the drug concentration in blood. The total concentration of FK506 in transplanted patients' blood must be kept between 5 and 20 ng mL^{-1} to maximize efficacy and minimize its side effects.^[8] Moreover, this molecule displays a very narrow therapeutic window,^[9] further increasing the interest of developing (immuno)biosensors for POCT.^[10] However, the drug hydrophobicity makes it a strong binder to serum proteins so that the FK506 free fraction amounts to less than 0.5% of the total concentration in whole-blood, a very relevant fact since its toxicity might be related to the unbound fraction.^[11] This is an additional nuisance if microdialysis sampling for subsequent analysis is desired.^[12]

Tacrolimus analysis in blood by immunoassays currently include enzyme-linked type (ELISA),^[13] microparticle enzyme-linked immunoassays,^[14] without or within a microfluidic device,^[15] antibody-conjugated magnetic immunoassays,^[16] and chemiluminescent enzyme immunoassays (CLIA).^[17] All these methods require several steps and the use of reagents to quantify the binding event (either an enzymatic reaction in ELISA, or a chemiluminescent reaction in CLIA). The advantage of the latter two is their high sensitivity; however, for (semi)continuous monitoring, it would be desirable to have a method that operates directly without the need of a revealing step.

Because fluorescence-based methods are extremely responsive (down to single photon or single molecule detection) and relatively easy to perform, they are ideally suited to analytical applications that require high sensitivity and continuous monitoring.^[18] In this paper we describe a novel versatile approach for the determination of low drug levels by pooling at the same time all of the strategies mentioned above, namely, highly fluorescent dyes in the NIR region, embedded into magnetic nanobeads for signal amplification through fluorophore and particle accumulation, and combined with a Förster resonance energy transfer (FRET) between the dyes to achieve a large spectral separation between the excitation light and the fluorescence readout.

2. Results and Discussion

2.1. Fluorescent Labels

A suitable scaffold to build very brilliant dyes that combine a high fluorescence quantum yield with a strong absorption of

light is the boron-dipyrromethene ("BODIPY") chromophore (Scheme 1).^[19] The simplest BODIPY core displays absorption and emission bands centered at ≈ 500 and 510 nm, respectively, with fluorescence quantum yields approaching unity and absorption coefficients (ϵ) close to $10^5 \text{ L mol}^{-1} \text{ cm}^{-1}$.^[19] The versatile chemistry of BODIPY dyes allows introduction of additional π -conjugated units, with the consequent bathochromic shift of the absorption and emission bands while maintaining its strong fluorescence largely intact.^[20] This is an important feature to prepare fluorescent labels that operate in the near infrared region of the electromagnetic spectrum (650–900 nm) where interference from the light scattering is at its lowest. In addition, BODIPYs are insensitive to the solvent polarity and pH (unless they bear ad-hoc substituents), display sharp excitation and emission peaks contributing to increase their brightness, have a significant photochemical stability, and possess good solubility in many organic solvents.

A relevant drawback of BODIPY dyes for fluorescent labeling is their very small Stokes shifts (typically 10–20 nm), making it difficult to suppress the interference from the excitation light scattering. This is particularly relevant to the design of immunoassays on chip platforms, a format that usually employs laser excitation sources and plastic materials. An elegant way to circumvent this problem is the realization of intramolecular FRET dyads or "cascades," in which the excitation energy can be transferred from one BODIPY dye to a second one (or more), displaying a larger virtual Stokes shift. FRET is also possible between donor and acceptor molecules encapsulated into nanoparticles.^[3b,21] The hydrophobic nature of BODIPY dyes allows their straightforward immobilization into latex (polystyrene) beads by swelling them in an organic solvent in the presence of the dye and subsequent shrinking.^[22] Additionally, if the selected polystyrene beads include a magnetic core or are decorated with ferrite nanograins, they will enable their concentration onto the detection region, facilitating also the incubation–separation procedures required in any immunoassay.

For preparing our fluoromagnetic nanobeads, we first proceeded with the selection of the fluorophores for encapsulation. Taking into account their very apt properties discussed above, we designed two BODIPY dyes for intraparticle FRET (Scheme 1), i.e., a perfluoro BODIPY donor (PFB-515) and an acceptor (PFB-641) one, the latter with a π -extended scaffold for absorption and emission in the NIR region. The donor (D) and acceptor (A) dyes incorporate a

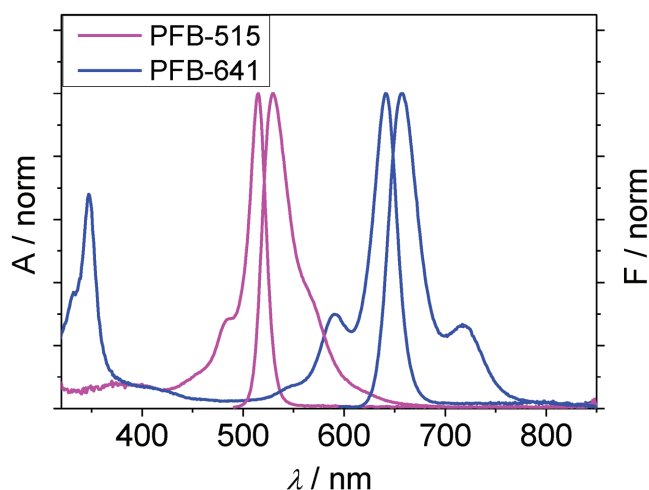


Figure 1. Normalized absorption and fluorescence of PFB-515 (pink; $\lambda_{\text{ex}} = 485$ nm) and PFB-641 (blue; $\lambda_{\text{ex}} = 590$ nm) in EtOH ($c_{\text{dye}} = 1 \mu\text{M}$).

pentafluorophenyl substituent in the *meso* position. Such highly electron withdrawing unit confers BODIPY dyes a higher fluorescence quantum yield, longer emission lifetime, and bathochromic shifts in absorption and emission maxima with respect to the parent *meso*-phenyl derivative.^[23] To accomplish an efficient FRET process, we also have to keep in mind that the selected dyes must display the largest possible spectral overlap between the emission of D and the absorption of A.

The PFB-515 and PFB-641 boron-dipyrromethene dyes were synthesized following similar procedures to those described in the literature (Scheme 1).^[24] After chromatographic purification, the dyes were spectroscopically characterized to verify their fitness-to-purpose (Figure 1 and Table 1). The typical π - π^* absorption and emission maximums of BODIPY dyes appear at 515 and 525 nm, respectively, for PFB-515 in ethanol, with a remarkable fluorescence quantum yield ($\Phi_f = 0.87$) and a rather long decay time (6.2 ns) for this type of dyes due to the electron-withdrawing effect of the perfluorinated phenyl ring. In the same solvent, PFB-641 shows maximums at 641 nm (absorption) and 657 nm (emission), a Φ_f of 0.73, and a fluorescence lifetime of 4.0 ns, a lower value than that of PFB-515 due to the much smaller excited state–ground state energy gap of the former.

Figure 1 demonstrates the significant spectral overlap between the emission of PFB-515 and the absorption of PFB-641. In order to calculate it and, in this way, how effective the FRET process results, the spectral overlap integral $J(\lambda)$ and the Förster distance (R_0 , also called “critical quenching radius,” namely, the donor–acceptor distance at which the probability of the excited donor to fluoresce is equal to the probability of energy transfer to the acceptor) were determined using Equations (1) and (2)^[25]

$$J(\lambda) = \int_0^\infty F_D(\lambda) \varepsilon_A(\lambda) \lambda^4 d\lambda = \frac{\int_0^\infty F_D(\lambda) \varepsilon_A(\lambda) \lambda^4 d\lambda}{\int_0^\infty F_D(\lambda) d\lambda} \quad (1)$$

Table 1. Photophysical data of the BODIPY dyes (1 μM) in air-equilibrated ethanol at 25 °C.

Dye	$\lambda_{\text{abs}}^{\text{max}}$ [nm] ^{a)}	ε_{max} [$\text{M}^{-1} \text{cm}^{-1}$]	$\lambda_{\text{em}}^{\text{max}}$ [nm] ^{a)}	$\Phi_f^{\text{d)}$	τ [ns] ^{e)}
PFB-515	515	6.0×10^4 ^{b)}	525	0.87	6.2
PFB-641	641	9.4×10^4 ^{c)}	657	0.73	4.0

^{a)} $\lambda \pm 0.5$ nm; ^{b)} $\varepsilon \pm 3000 \text{ M}^{-1} \text{cm}^{-1}$; ^{c)} $\varepsilon \pm 12\,000 \text{ M}^{-1} \text{cm}^{-1}$; ^{d)} Fluorescence quantum yields determined using rhodamine 123 ($\Phi_f = 0.90$ in EtOH ($\lambda_{\text{ex}} = 485$ nm)^[41]) and oxazine 170 ($\Phi_f = 0.579$ in EtOH, $\lambda_{\text{ex}} = 610$ nm)^[42] as reference dyes for PFB-515 and PFB-641, respectively; the uncertainty in the Φ_f determination is below 5%; ^{e)} ± 0.1 ns.

$$R_0/n\text{m} = 2.108 \times 10^{-2}$$

$$\left\{ \kappa^2 \Phi_D^0 n^{-4} \int_0^\infty F_D(\lambda) [\varepsilon_A(\lambda) / \text{dm}^3 \text{mol}^{-1} \text{cm}^{-1}] (\lambda/n\text{m})^{-4} d\lambda \right\}^{1/6} \quad (2)$$

In Equation (2), κ is the dipole orientation factor (which is usually assumed to be equal to $(2/3)^{1/2}$ for randomly oriented transition dipole moments of the dyes), Φ_D^0 is the fluorescence quantum yield of the donor in the absence of acceptor, N is the Avogadro’s number, n is the average refractive index of the medium in the wavelength range where the spectral overlap occurs, $F_D(\lambda)$ is the normalized spectral fluorescence radiant intensity of the donor so that $\int_0^\infty F_D(\lambda) d\lambda = 1$, and $\varepsilon_A(\lambda)$ is the molar decadic absorption coefficient of the acceptor at λ .

The calculated overlap integral for our D/A pair in ethanol ($n = 1.3611$ ^[26]) is $1.35 \times 10^{15} \text{ M}^{-1} \text{cm}^{-1} \text{nm}^4$, yielding a Förster distance of 5.2 nm, a similar value for instance to those reported for the popular fluorescein isothiocyanate–tetramethylrhodamine FRET pair (4.9–5.4 nm).^[27] The energy transfer rate, $k_T(r)$, is given by $1/\tau_D$ when the D-to-A distance (r) is equal to R_0 . Therefore, when the energy transfer efficiency is 50%, k_T amounts to $1.6 \times 10^8 \text{ s}^{-1}$.

2.2. Fluorescent Doping of Magnetic Nanoparticles (NPs)

Commercial carboxylated magnetic nanospheres (Estapor, Merck Millipore) of 300 nm diameter (as per dynamic light scattering measurements from the manufacturer), were selected as the nanoparticle platform suitable for immunoassays (300 nm was a compromise between large enough particles for significant magnetic attraction, but small enough to keep a good surface-to-volume ratio). The Estapor polystyrene nanospheres are decorated with $\approx 55\%$ (by weight) of ferrite nanograins (≈ 8 – 10 nm size, as shown by transmission electron microscopy, Figure 2) that confer them superparamagnetic properties. Carboxylic functionalization of the NPs surface (148 $\mu\text{eq CO}_2\text{H/g}$) was chosen to allow facile bioconjugation with the detection (IgG anti-IgM) antibodies (see Section 2.5).

For fluorescent doping of the NPs, optimization of the dye loading was performed in the first place. The magnetic beads were loaded with either PFB-515 or PFB-641, and different batches were prepared by increasing the concentration of each dye in the loading solution. According to the method we have developed, the commercial aqueous suspension of magnetic particles is first diluted with water and then tetrahydrofuran (THF) is added to swell the polystyrene core. Swelling allows easy diffusion of the hydrophobic dyes into the polystyrene matrix

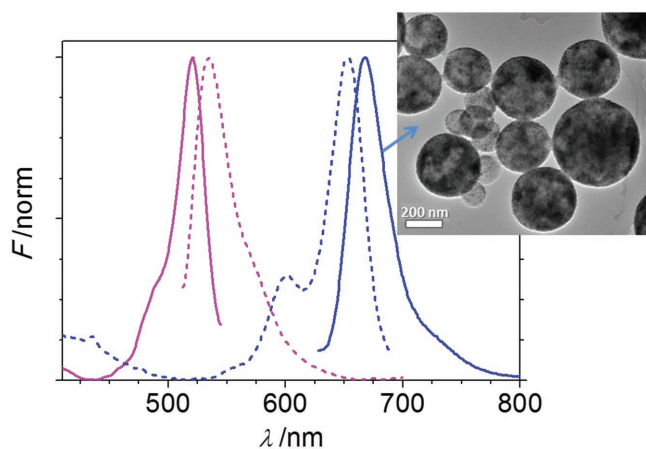


Figure 2. Excitation and emission spectra of suspensions of magnetic nanoparticles doped with either PFB-515 (3.2 nmol dye/mg NPs; $\lambda_{\text{ex}} = 495$ nm, $\lambda_{\text{em}} = 570$ nm, in pink color) or PFB-641 (3.0 nmol dye/mg NPs; $\lambda_{\text{ex}} = 590$ nm, $\lambda_{\text{em}} = 715$ nm, in blue color) in water. The inset shows a TEM image of the PFB-641-doped magnetic nanoparticles (batch “b” of Table 2).

outermost surface. Immediately after, a THF solution of the corresponding PFB dye is added. After vortex stirring, the particles are thoroughly washed with water with the aid of a neodymium magnet to keep them in the tube, and resuspended in the same solvent. Although the amount of PFB dye was varied for the different batches, the total amount of THF was always kept at 250 μL per mL of water in order to ensure reproducible swelling of the polystyrene fluoromagnetic nanoparticles (FMNPs).

As shown in Figure S1 in the Supporting Information for FMNPs containing PFB-641 (this study was only performed with the acceptor dye), an increase of the dye loading yields a small red shift of its emission maximum, together with a decrease of its fluorescence lifetime. The emission red shift

might be attributed to the fact that a larger number of dye molecules per FMNP leads to stronger inner-filter effect due to the very small Stokes shift of the dye, apparently moving up its fluorescence maximum.^[28] The same effect is observed upon increasing the dye concentration in solution. The fluorescence intensity of the FMNPs levels off at ≈ 5 nmol of PFB-641 per mg of MNPs (Figure S1c, Supporting Information).

Table 2 shows the emission lifetimes measured for different batches of fluorescent NPs in aqueous suspension. Although the emission decay of the free dyes in ethanol is purely exponential, the fluorescence decay of the NPs always obeyed multiexponential kinetics. To be able to compare the different systems, we calculated the so-called preexponentially weighted fluorescence lifetimes (τ_m , Table 2).^[29] Calculation of τ_m allows a more robust comparison of heavily nonexponential decays, as it removes the uncertainty of the parameters of the fit (preexponential factors and lifetimes) caused by their important covariance.^[30] The robustness of τ_m lies on the fact that it is also equal to the area under the decay curve divided by the y -intercept, so that it is independent of any fit.^[31]

The τ_m of the FMNPs doped with PFB-641 ($\lambda_{\text{ex}} = 640$ nm; $\lambda_{\text{em}} = 680$ nm) decreases from 1.97 to 1.29 ns as the concentration of the fluorophore increases (Table 2), being those values always lower than the emission lifetime of the free dye in ethanol diluted solution (4.0 ns). The same effect is also evident in the case of the MNPs loaded with PFB-515 ($\lambda_{\text{ex}} = 463$ nm; $\lambda_{\text{em}} = 550$ nm): τ_m decreases from 2.16 to 1.85 ns upon an increase of the immobilized dye concentration (6.2 ns for the dye in solution). The emission lifetime decline after immobilization and upon increasing the immobilized dye concentration is in agreement with the changes observed by other authors: when a high number of fluorophores are encapsulated into an NP, the high local concentration of dyes favors formation of short-lived fluorescent aggregates.^[3b] Moreover, the observed concentration quenching might be due to the Fe_3O_4 grains embedded into the polystyrene surface. It has

Table 2. Fluorescence lifetimes of different batches of dye-loaded magnetic nanoparticles in aqueous suspension at $(25 \pm 1)^\circ\text{C}$.

Batch	PFB-515/-641 [10^{-9} mol ^{a)}]	$\lambda_{\text{ex}}/\lambda_{\text{em}}$ [nm]	τ_1 [ns] (% B_1) ^{b)}	τ_2 [ns] (% B_2) ^{b)}	τ_3 [ns] (% B_3) ^{b)}	τ_m [ns] ^{c)}
FMNP-641a	-/1.5	640/680	0.61 (34.7)	2.60 (62.4)	4.86 (2.9)	1.98
FMNP-641b	-/3.0	640/680	0.87 (50.6)	2.66 (49.0)	7.67 (0.4)	1.77
FMNP-641c	-/6.0	640/680	0.44 (36.7)	1.69 (41.6)	3.16 (21.7)	1.55
FMNP-641d	-/7.5	640/680	0.45 (39.0)	1.72 (49.6)	3.30 (11.3)	1.40
FMNP-641e	-/9.0	640/680	0.47 (52.8)	1.94 (41.5)	3.84 (5.8)	1.27
FMNP-641f	-/12	640/680	0.42 (43.5)	1.69 (47.4)	3.37 (9.1)	1.29
FMNP-641g	-/15	640/680	0.43 (37.4)	1.73 (51.7)	3.31 (10.9)	1.41
FMNP-515a	3.2/-	463/550	0.93 (59.8)	3.81 (39.6)	15.7 (0.6)	2.16
FMNP-515b	4.8/-	463/550	0.68 (64.7)	3.57 (32.8)	9.61 (2.5)	1.85
FMNP-ETa	4.8/4.8	463/550	0.53 (85.6)	4.43 (13.8)	17.2 (0.5)	1.16
FMNP-ETa	4.8/4.8	463/680	1.02 (52.1)	2.79 (47.7)	16.1 (0.2)	1.89
FMNP-ETb	6.4/3.2	463/550	0.67 (84.2)	4.30 (15.2)	16.1 (0.6)	1.32
FMNP-ETb	6.4/3.2	463/680	1.27 (45.1)	3.01 (54.7)	18.4 (0.2)	2.25

^{a)} Moles of dye per mg of MNPs (dry weight); ^{b)} $I_f(t) = A + \sum_{i=1}^3 B_i \exp(-t/\tau_i)$, where $\%B_i = B_i \times 100 / \sum_{i=1}^3 B_i$; ^{c)} $\tau_m = \sum_{i=1}^3 B_i \tau_i / 100$.

been demonstrated that nanoparticulated Fe_3O_4 is an efficient quencher of the BODIPY fluorescence by photoinduced electron transfer from the excited state of the latter to an unfilled d orbital of the Fe^{III} atoms of the metal oxide.^[32] Therefore, the higher the concentration of surface-embedded dye, the larger the number of molecules next to the surface Fe_3O_4 nanograins leading also to the observed fluorescence lifetime quenching.

Excitation and emission spectra in water for the particles loaded with PFB-515 or PFB-641 are shown in Figure 2. As discussed above, compared to the free dyes in diluted ethanol solution (Table 1), the spectral maxima of the FMNPs are considerably red shifted in all cases. For example, $\lambda_{\text{abs}}/\lambda_{\text{em}}$ are 515/525 nm for PFB-515 in ethanol but 521/535 nm for the FMNPs doped with PFB-515 at 6.4 nmol mg^{-1} MNPs; $\lambda_{\text{abs}}/\lambda_{\text{em}}$ are 641/657 nm for PFB-641 in ethanol but 653/668 nm for FMNPs doped with PFB-641 at 3.0 nmol mg^{-1} MNPs. Because the absorption and emission maxima are red shifted synchronously upon immobilization, the D–A spectral overlap is also large for an efficient FRET into the dye-doped NPs. Therefore, we should observe sensitized emission of PFB-641 at $\lambda > 650$ nm by exciting the donor PFB-515 around 500 nm. In this way, a virtual Stokes shift larger than 150 nm can be achieved so that suppression of the disturbing scattering effects and, consequently, enhancement of the immunoassay sensitivity should be feasible. In order to confirm these predictions, magnetic NPs doped with mixtures of PFB-515 and PFB-641 were prepared. It is important to mention that both dyes are readily coencapsulated into the polystyrene matrix because they have similar polarity.

2.3. Preparation of the FRET Magnetic NPs (MNPs)

The Estapor magnetic nanoparticles were simultaneously doped with PFB-515 and PFB-641 for obtaining the sought intraparticle FRET system. The proper acceptor dye concentration was determined as described above for the PFB-641-doped FMNPs to find out that ≈ 5 nmol of PFB-515 per mg of MNPs provided the maximum emission intensity. Keeping constant the total amount of immobilized dye molecules at ≈ 10 nmol mg^{-1} MNPs, the PFB-515 to PFB-641 mole ratio was varied from 1:1 to 2:1 in order to investigate the effect of the relative amount of A with respect to D; the results are shown in Figure S2 in the Supporting Information. In spite of the smaller number of A molecules, we can observe that an increase of the D/A ratio leads to higher fluorescence from the acceptor dye, meaning that the FRET process is improved due to the presence of more “antennas.” This enhancement is confirmed in the excitation spectra (Figure S2, Supporting Information) and in the study of the fluorescence lifetimes (see below). Therefore, a 2:1 D/A mole ratio was chosen for preparation of the optimized FRET-based MNPs that were finally used for the bioconjugation.

Next, two D/A ratios were tested to confirm the improved FRET efficiency in the FMNPs (Table 2). To determine the emission lifetimes of the latter, the same excitation wavelength was always employed (463 nm, absorption of the donor), while the fluorescence was monitored at two different wavelengths (550 nm emission from D or 680 nm emission from A). In

every case, and although the fluorescence lifetime of PFB-641 is shorter than that of PFB-515 (4.0 and 6.2, respectively, see above), the lifetimes measured at 680 nm (1.89 and 2.25 ns for D/A 1:1 and 2:1, respectively) are longer than those measured at 550 nm (1.16 and 1.32 ns for D/A 1:1 and 2:1, respectively) (Table 2), indicating the occurrence of the FRET process. These results confirm that a higher relative amount of donor dye (D/A 2:1 vs 1:1) leads to a longer-lived acceptor species, suggesting a more efficient FRET quenching and lending support to the results of the fluorescent intensity measurements discussed above.

2.4. Coupling of Capture Antibodies to the Fluoromagnetic Nanoparticles

The selected FRET-based fluoromagnetic nanoparticles (FMNP-ETb, Table 2) were conjugated to different capture antibodies after activation of the former with the classical 1-ethyl-3-(3-(dimethylamino)propyl)carbodiimide (EDC)/sulfo-*N*-hydroxysuccinimide (NHS) combination in 2-(*N*-morpholino)ethanesulfonic acid hydrate (MES) buffer (Figure 3). Then, they were washed with phosphate-buffered saline StartingBlock™ blocking buffer containing sodium dodecylsulfate (PBSSDS) and incubated in the same buffer with the required capture antibody to Tacrolimus. Additionally, some FMNPs were functionalized with neutravidin to be used as positive or negative control in the immunoassays. Efficient conjugation of the IgG anti-IgM antibodies to the fluoromagnetic NPs was confirmed by a magnetic bead-based enzymatic assay,^[33] using a microplate fluorescence reader, horseradish peroxidase (HRP)-labeled anti-IgG, and the commercial Amplex Red Hydrogen Peroxide/Peroxidase Assay Kit (Figure S3, Supporting Information). The very small response obtained for FMNPs coated with neutravidin (negative control) confirms the selectivity of the assay.

2.5. FMNPs-Based Competitive Immunoassay for Tacrolimus

Determination of the immunosuppressant used to test the FRET-based fluoromagnetic nanoparticles is based on a competitive (inhibition) assay between a suitable derivative of Tacrolimus (FK506- CO_2H) immobilized onto the glass bottom surface of the microwells, and Tacrolimus present in the sample, for a limited number of antibody (Ab) binding sites (Figure 4). In order to achieve a defined and sufficiently high density of immobilized haptens without loss of their biological activity, the glass wells were functionalized with either 3-aminopropyltriethoxysilane (APTES) or poly-L-lysine. Figure S4 in the Supporting Information shows that the latter provides significantly lower background (measured in the absence of anti-FK506 antibody) while the fluorescence is high and reproducible, so that it was selected for further experiments.^[34]

The fluorescence data were plotted as the *B* (fluorescence signal in the presence of FK506) to *B*₀ (fluorescence signal in the absence of the analyte) ratio against the FK506 concentration on a logarithmic scale (Figure 5). The experimental points

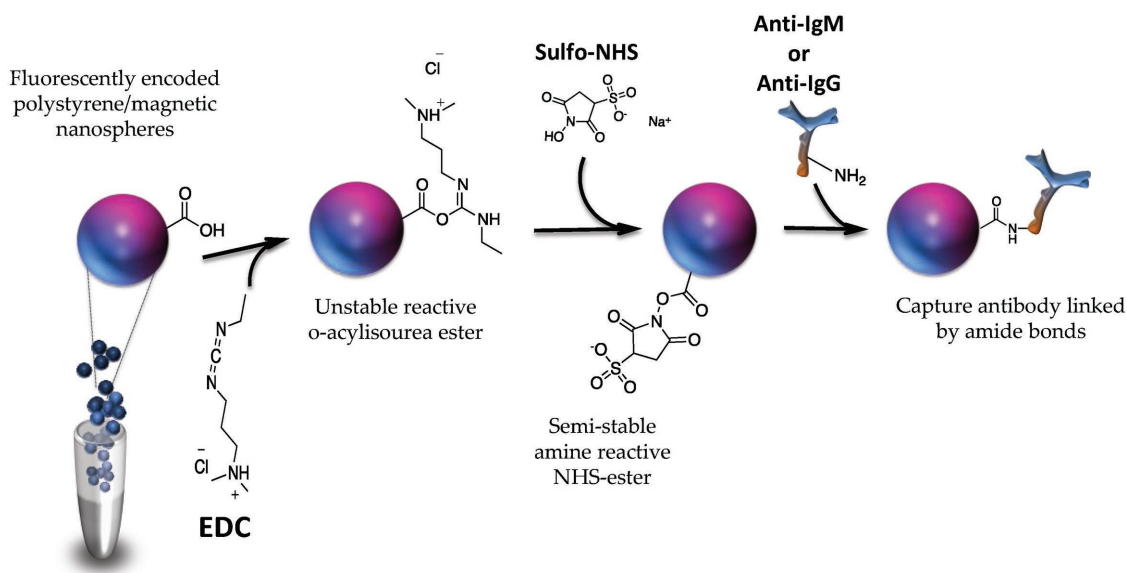


Figure 3. Workflow of the protocol followed to couple the carboxylated fluorescent magnetic nanoparticles to the detection antibodies using the EDC/sulfo-NHS method.

are fitted (Systat Sigma Plot v.12) to a four-parameter sigmoidal logistic equation (Equation (3))^[35]

$$\frac{B}{B_0} = \frac{A_{\max} - A_{\min}}{1 + \left(\frac{[\text{FK506}]}{\text{IC}_{50}}\right)^b} + B_{\min} \quad (3)$$

where A_{\max} and A_{\min} are the asymptotic maximum and minimum of the normalized signal, respectively, b represents the slope of the curve at the inflection point, and IC_{50} is the concentration of analyte at the inflection point (concentration giving 50% inhibition of A_{\max}). The LOD was calculated as the analyte concentration for which the tracer binding to the antibody is inhibited by 10%, and the dynamic range of the method corresponds to the analyte concentrations that produce a normalized response in the 20–80% range.

Figure 5 shows the competitive inhibition curves obtained using FK506 standard solutions in the 0.01–7500 ng mL⁻¹ range. When the signal was acquired in the FRET mode, i.e., upon excitation at the donor absorption wavelength (525 nm) and monitoring the sensitized emission of the acceptor at 680 nm, the LOD and IC_{50} values obtained were 0.08 and 0.47 ng mL⁻¹, respectively, with a dynamic range of 0.15–2.0 ng mL⁻¹. However, when the direct excitation mode was used, i.e., by illuminating at the acceptor absorption (638 nm) and monitoring its fluorescence at 680 nm (without any FRET), the signal background was found to be significantly higher. Thus, both the LOD (0.27 ng mL⁻¹) and the IC_{50} value (23 ng mL⁻¹) were higher, with a dynamic range between 4.1 and 130 ng mL⁻¹.

The last recommendation of a panel of European experts on Tacrolimus is the development of analytical methods featuring a limit of quantification up to 1 ng mL⁻¹ in order to provide reliable concentrations during low-dose Tacrolimus therapy.^[36] In this context, the proposed system would be sensitive enough to quantify Tacrolimus in real samples given its insensitivity to the

sample fluorescence background. Even more, compared to previously reported fluoroimmunoassays for Tacrolimus, the novel FRET-based fluoromagnetic nanoparticles showed similar^[37] or superior^[38] performance in terms of sensitivity.

3. Conclusion

Carboxylated polystyrene nanoparticles decorated with ferrite nanograins have been successfully doped with highly fluorescent BODIPY dyes using a simple straightforward protocol. The particles have been produced either with i) a single BODIPY dye, suitable for excitation with a 532 nm green laser diode or for excitation in the red (e.g., 635 nm), or ii) with a mixture of both BODIPY dyes to obtain an efficient FRET that allows for a virtual Stokes shift larger than 150 nm. The resulting doped fluoromagnetic nanoparticles (≈ 300 nm diameter) are stable in water and the dyes do not leach out of the polystyrene matrix in aqueous buffered solution. They are significantly brilliant, a remarkable feature taking into account the brown-colored ferrite layer that covers its polystyrene core. The presence of $-\text{CO}_2\text{H}$ groups on the surface allows further bioconjugation, demonstrated with a successful immunoassay for the immunosuppressive Tacrolimus drug based on nanoparticle-bound IgG anti-IgM antibody as detection probe. The assay sensitivity significantly improves when measuring in the FRET mode with excitation in the blue–green and fluorescence detection in the near infrared, compared to the same nanoparticle-based immunoassay carried out in conventional fluorescence mode (even with excitation in the red at 638 nm). Additionally, more than two dyes with suitable absorption/emission features might be loaded into the nanoparticles to perform FRET “cascades” with an even larger virtual Stokes shift. The novel FRET-based fluoromagnetic nanoparticles pave the way to develop point-of-care-testing immunobiosensors on a chip due to the stringent requirements of the latter (small volume, analysis turnover

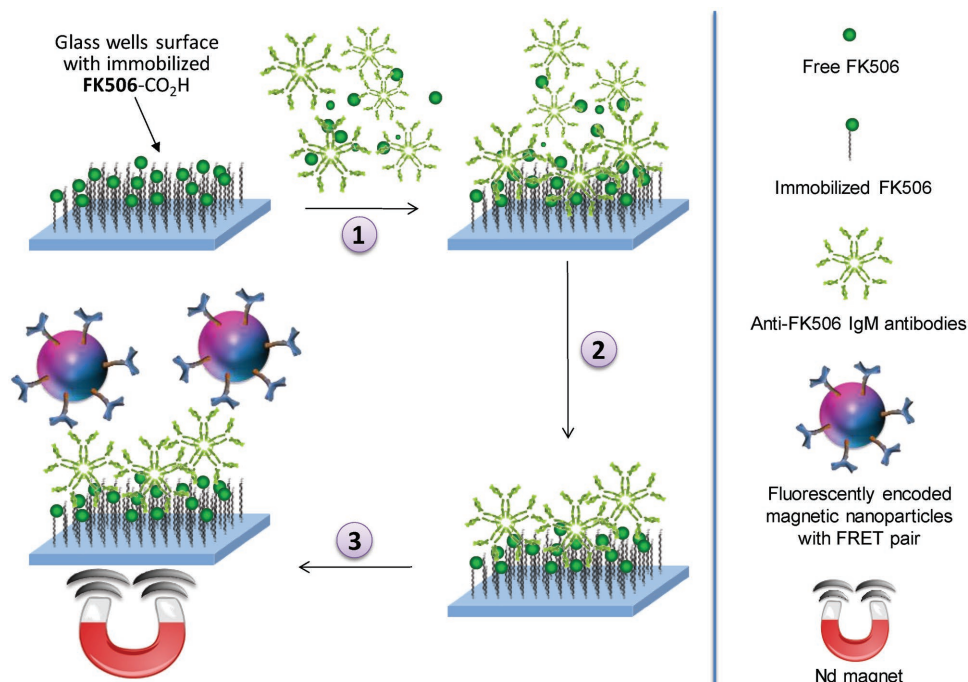


Figure 4. Tacrolimus immunoassay protocol summary: 1) mixing and incubation of sample and IgM anti-FK506 antibody into (FK506-CO₂H)-bound microwell; 2) wash out of the bioreagents excess; 3) incubation with FMNP-ETb functionalized with the detection IgG anti-IgM antibody, second wash, and fluorescence measurement.

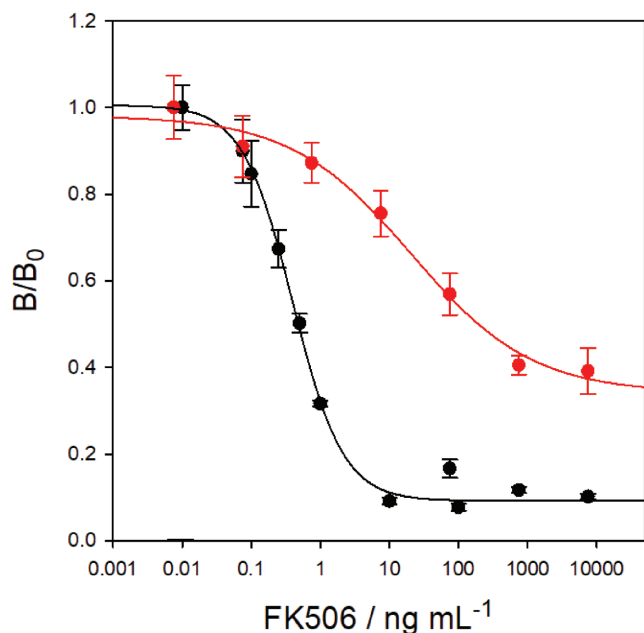


Figure 5. Competitive immunoassay calibration curve. The plate was assayed with FK506 (0 and 0.010 to 7500 ng mL⁻¹) in the presence of 2.5 μg mL⁻¹ of anti-FK506 and 2.5 μg mL⁻¹ of anti-biotin (positive control) antibodies. Tracer solution is a mixture of 3 μg mL⁻¹ of fluorescently encoded magnetic nanoparticles decorated with either anti-IgM or anti-IgG (positive control) ($n = 3$). Results obtained when the FMNPs were excited at the 525 nm donor absorption (in black), or when the FMNPs were directly excited at the 638 nm FPB-641 absorption (in red). In both cases, fluorescence was monitored at 680 nm.

time, low background for laser interrogation, chip and optical fiber materials, etc.).^[39]

4. Experimental Section

Materials: All reagents were provided by commercial suppliers and used without further purification. Pentafluorobenzaldehyde (≥98%) was from Alfa Aesar; 2,4-dimethyl-1H-pyrrole (97%), tetrachloro-*p*-benzoquinone (chloranil) (99%), boron trifluoride diethyl etherate (≥46.5%) solution, dichloromethane (synthesis grade), benzaldehyde (98%), and piperidine (99%) were from Acros Organics; triethylamine (≥99%) was from Riedel-de Haën, and trifluoroacetic acid and toluene were from Sigma-Aldrich. The magnetic nanospheres (Estapor, Merck Millipore), supplied as aqueous suspension with a solid content of 10% by weight, have a mean diameter of 301 nm (manufacturer value obtained by dynamic light scattering), a magnetite content of 54.1% w/w (dry weight), and a concentration of -CO₂H surface groups of 148 μeq g⁻¹. Tacrolimus (FK506, +98%) was provided by Sinoway Ind. Co. (China). EDC, NHS, MES, D-biotin, APTES, and poly-L-Lysine 0.1% w/v were from Sigma-Aldrich. HPLC-grade ethanol was supplied by Panreac Quimica. Phosphate-buffered saline (PBS, 100 × 10⁻³ M), molecular biology grade water, sodium dodecyl sulfate solution (SDS, 20%), and Tween-20 (T20) were purchased from Sigma-Aldrich and sodium hydroxide solution (5N, certified) was from Fisher Scientific. PBS Protein-free blocking buffer, PBS StartingBlock blocking buffer (PBSS), TBS StartingBlock blocking buffer (TBSS) were from Thermo Scientific. PBSSDS buffer was prepared with 100 × 10⁻³ M PBS, 100 × 10⁻³ M NaCl, and 0.01% SDS, at pH 7.2; PBSTM buffer was prepared with 10 × 10⁻³ M PBS, 0.05% T20, and 0.3% w/v of powdered defat milk, at pH 7.4. Mouse monoclonal immunoglobulin M (IgM) and antibodies raised against FK506 (anti-FK506 Ab) were supplied by Santa Cruz Biotechnology. IgG fraction monoclonal mouse against biotin (anti-biotin Ab), affinity-purified rabbit anti-mouse IgG, and affinity-purified donkey antimouse IgM antibodies were purchased from Jackson

ImmunoResearch. Biotin and Tacrolimus stock solutions were prepared in dimethylsulfoxide (1 mg mL⁻¹) and stored at -20 °C. Tacrolimus standard solutions for calibration purposes were prepared daily upon dilution of the stock solutions in PBS (10 × 10⁻³ M, pH 7.4). Water was purified with a Direct-Q3-UV system (Merck Millipore). 96-well glass-bottom MatriPlates (630 µL per well) black plates were from GE Life Sciences (Pittsburgh, PA).

Instrumentation: ¹H NMR spectra were recorded on a Bruker Avance DPX 300MHz-BACS60 spectrometer (UCM Central Instrumentation Facilities). NMR chemical shifts were expressed relative to the signals of the nondeuterated traces of the solvent (CDCl₃ at 7.24 ppm). Mass spectra were obtained either with a Bruker HCT Ultra (ESI) or an ULTRAFLEX matrix-assisted laser desorption/ionization-time of flight (MALDI-TOF/TOF) spectrometer (UCM Central Instrumentation Facilities). Transmission electron microscopy measurements were carried out with a JEOL JEM 2100 (200 kV) at the ICTS Centro Nacional de Microscopía (Madrid, Spain). UV-vis absorption spectra were recorded with a Varian Cary 3-Bio spectrophotometer. Steady-state emission measurements were carried out on a Horiba Fluoromax-4TCSPC spectrofluorometer equipped with a 150 W xenon lamp for the steady-state spectral recordings. For time-resolved fluorescence determinations, either a Horiba Fluoromax-4TCSPC instrument or a FLS980 fluorescence spectrometer (Edinburgh Instruments, with double monochromator in the emission channel) were employed. In both cases, a Horiba NanoLED-470LH laser diode (463 nm, 1 ns pulses) for PFB-515, and Horiba NanoLED-635L laser diode (peak at 640 nm, 250 ps pulses) for PFB-641 were used. In the case of the Fluoromax-4TCSPC, the emitted light was filtered through 475 and 495 nm long-pass filters for the PFB-515 dye, and through a 665 nm long-pass filter for the PFB-641 fluorophore. Fluorescence decays were measured with a 50, 100, or 200 ns window (4096 channels), after accumulating at least 20 000 counts in the peak channel, with a 500 kHz repetition rate. Emission lifetimes were extracted from the exponential curve fittings using the proprietary Horiba or Edinburgh Instruments algorithms (with deconvolution of the instrumental response function). Any observed decay component equal to or below the laser pulse width was discarded. The goodness-of-the-fit of the exponential decays was judged by visual inspection and the reduced chi-squared parameter ($\chi_r^2 < 1.5$) of the residuals. All emission measurements were carried out under air using optically diluted samples ($A_{\max} < 0.1$). For fluorescence-based immunoassays in a microplate, a fluorescence reader (CLARIOstar, BMG Labtech) was employed; instrument control and data processing were performed with the manufacturer original software (MARS).

Synthesis of PFB-515 (4,4-difluoro-1,3,5,7-tetramethyl-8-pentafluorophenyl-4-bora-3a,4a-diaza-s-indacene): 647 mg of pentafluorobenzaldehyde (3.30 mmol) and 924 mg of 2,4-dimethyl-1H-pyrrole (9.71 mmol) were dissolved in CH₂Cl₂ (5 mL) under argon. Then a few drops of trifluoroacetic acid were added. The reaction mixture was kept in the dark and stirred for 4 h at room temperature until the aldehyde was consumed (monitored by thin-layer chromatography (TLC)); In the next step, oxidation of the intermediate was performed by adding 789 mg of tetrachloro-*p*-benzoquinone (chloranil) (3.21 mmol) dissolved in CH₂Cl₂ (30 mL). The reaction mixture was stirred for 1 h. Finally, 6.63 mL of a solution of boron trifluoride diethyl etherate (52.33 mmol) were added together with 6.46 mL of triethylamine (46.35 mmol). The reaction was stirred for two additional hours. The crude reaction mixture was washed with H₂O and extracted with CH₂Cl₂, the organic phase was dried with MgSO₄ and the solvent was removed under reduced pressure. The crude product was first purified with flash column chromatography on silica gel (hexane-ethylacetate with 15:1 to 9:1 v/v gradient) and then on neutral aluminum oxide (hexane-ethyl acetate with 33:1 to 18:1 v/v gradient). PFB-515 was obtained as orange crystals with a green glow (205.0 mg, 15% yield). $\lambda_{\text{abs}} = 515$ nm (EtOH); ¹H NMR (Figure S5 (Supporting Information); 300 MHz, CDCl₃, δ): 1.62 (s, 6H, CH₃), 2.57 (s, 6H, CH₃), 6.06 (s, 2H). ¹⁹F NMR (Figure S6 (Supporting Information); 282 MHz, CDCl₃; δ from CFC1₃): -140.33 (dd, 2F, ³J = -21.5 Hz; ⁴J = 7.1 Hz), -146.84 (q, 2F, ¹J_{F-B}(^{app}) = 32.0 Hz), -151.56 (t, 1F, ³J = -19.7 Hz), -160.58 (m, 2F). MS (ESI⁺) (Figure S7,

Supporting Information): m/z [M + Na]⁺ calcd. for [C₁₉H₁₄BF₇N₂ + Na]⁺, 437.103; found, 437.105.

Synthesis of PFB-641 (4,4-difluoro-1,7-dimethyl-3,7-distyryl-8-pentafluorophenyl-4-bora-3a,4a-diaza-s-indacene): 51.81 mg of PFB-515 (0.13 mmol), 0.040 mL of benzaldehyde (0.36 mmol), and piperidine 0.025 mL (0.26 mmol) were dissolved in anhydrous toluene (2 mL) under argon. The reaction mixture was refluxed for 24 h protected from light. The crude product was cooled to room temperature and the solvent was removed under vacuum. Purification was carried out by silica-gel column chromatography (hexane-dichloromethane with 1:0 to 2:1 v/v gradient). PFB-641 was obtained as a dark blue solid (6.81 mg, 13% yield). $\lambda_{\text{abs}} = 641$ nm (EtOH); ¹H NMR (Figure S8 (Supporting Information); 300 MHz, CDCl₃, δ): 1.57 (s, 6H, CH₃), 6.74 (s, 2H) 7.30–7.47 (m, 8H, CH_A, and CH=CH), 7.63–7.81 (m, 6H, CH_A, and CH=CH). MS (MALDI-TOF) (Figure S9, Supporting Information): m/z [M⁺] calcd. for C₃₃H₂₂BF₇N₂, 590.18; found, 589.99.

Once prepared, the dyes were stored in the solid state at 2 °C in the dark.

Synthesis of Carboxylated Tacrolimus: Carboxylated Tacrolimus (FK506-CO₂H) was prepared according to Cañadas et al.^[40] by reaction of commercial Tacrolimus with carboxymethoxyamine hemichlorhydrate in anhydrous methanol, in the presence of sodium acetate, as shown on Scheme S1 in the Supporting Information. Confirmation of the correct functionalization of Tacrolimus was provided by comparison of the corresponding ¹³C NMR spectra (Figures S10 and S11, Supporting Information) as well as from the mass spectrum of the carboxylated Tacrolimus (Figure S12, Supporting Information).

Fluorescent Doping of the Magnetic Nanoparticles: The carboxylated magnetic nanobeads were doped with either PFB-515 or PFB-641, and different batches with increasing dye concentrations were generated. In a general protocol, the commercial aqueous suspension of magnetic particles (100 µL) was diluted with water (900 µL) and then THF was added. Immediately after, a volume of the corresponding PFB dye solution in THF was incorporated. For the PFB-641 dye, 39, 78, 156, 195, or 234 µL of a 3.84 × 10⁻⁴ M stock (samples a to e), and 200 or 250 µL of a 6 × 10⁻⁴ M stock (samples f and g) were used; in the case of the FMNP-515 a and b samples, 67 or 125 µL of a stock solution of PFB-515 in THF ($c_{\text{stock}} = 3.85 \times 10^{-4}$ M) were added, respectively. The corresponding mixture was stirred in a vortex for 1 h at 600 rpm and, finally, the particles were washed three times with H₂O with the aid of a neodymium magnet to keep them on the tube wall, and resuspended in 1.7 mL of the same solvent. No fluorescence in the supernatant was detected after the third washing indicating the absence of dye leaching. The NP suspensions were stored at 4 °C in the dark. The amount of PFB dye was varied in the different batches, but the total amount of THF was always kept at 250 µL mL⁻¹ of H₂O in order to ensure a reproducible swelling of the polystyrene MNPs. The optimal dye concentration was determined for the PFB-641-doped FMNPs: ≈5 nmol dye per mg of NPs provided the maximum fluorescence intensity (Figure S1c, Supporting Information).

For preparing the FRET FMNPs, the Estapor beads were doped with both PFB-515 and PFB-641 dyes in a 1:1 or 2:1 (PFB-515/PFB-641) mole ratio. The optimal dye concentration was determined as described above for the PFB-641-doped FMNPs (≈5 nmol mg⁻¹ of FMNPs provided the maximum emission intensity). Keeping constant the total amount of immobilized dye molecules at 9.6 nmol dye per mg of MNPs, the following protocol for the MNPs doping was employed: a) 100 µL of the commercial MNP suspension ($c_0 = 100$ mg mL⁻¹) were diluted to 1 mL with water; b) after adding THF, the suspension was vigorously shaken for a couple of seconds; c) the corresponding volume of a stock solution containing already a mixture of the PFB dyes in THF was added (for the "FMNP-ETa" NPs, a 1:1 mixture containing 125 µL of PFB-515 dye + 125 µL of PFB-641 was added; for the "FMNP-ETb" NPs, a 2:1 mixture containing 167 µL of PFB-515 + 83 µL PFB-641 was used; in all cases, the $c_{\text{stock}}^{\text{PFB}}$ was 3.85 × 10⁻⁴ M); the total volume of THF was always kept at 250 µL mL⁻¹ H₂O; d) the mixture was shaken in a vortex for 3 h at 800 rpm; e) the FMNP suspensions were stored at 4 °C in the dark.

Coupling of the Fluoromagnetic Nanoparticles to Capture Antibodies: The selected magnetic FRET nanoparticles (FMNP-ETb, those doped

with a 2:1 PFB-515/PFB-641 mole ratio) were coupled to the different capture antibodies as follows: 50 μL of fluorescent nanoparticles suspension (containing approximately 0.2 mg of dry nanoparticles) was washed three times with 500 μL portions of MES buffer (0.1 M MES, 0.15 M NaCl, 0.01% SDS, pH 5.7). The nanoparticles were then activated in 1 mL of MES buffer containing 102×10^{-3} M EDC and 112×10^{-3} M sulfo-NHS for 2 h at room temperature in the dark. After activation, the microspheres were washed three times with 500 μL portions of PBSSDS buffer. Then they were incubated in 300 μL of PBSSDS buffer containing 60 μg of capture antibody (either anti-mouse IgM or anti-mouse IgG as positive control) for 4 h at room temperature in the dark. After incubation, the microspheres were washed three times with 500 μL portions of TBSS buffer, and blocked in 1 mL of TBSS buffer for 1 h at room temperature in the dark. After washing three times with 500 μL portions of TBSS buffer, the microspheres were stored in 100 μL of TBSS buffer at 4 $^{\circ}\text{C}$, protected from light. Additionally, another batch of magnetic nanoparticles were functionalized with neutravidin to be used as positive or negative control in the forthcoming experiments.

Functionalization of the Microwell Plates Bottom with Tacrolimus: The 96-well glass-bottom plates were previously cleaned with Alconox (Sigma-Aldrich), thoroughly washed with Milli-Q water, and rinsed with 96% ethanol. Then, 500 μL of a solution containing 2% APTES in ethanol-water (95:5, v/v) was added to each well and incubated for 1 h. The aminated slides were rinsed three times with clear ethanol and stored at 4 $^{\circ}\text{C}$ in the same solvent until use. In the case of poly-L-lysine coating, 500 μL of a solution containing poly-L-lysine 0.01% w/v in water was added to each well of the cleaned plates and incubated for 5 min. The coated slides were drained and dried at 60 $^{\circ}\text{C}$ overnight and stored at room temperature. FK506-CO₂H was immobilized onto the aminated surfaces by adding 200 μL of a 100 $\mu\text{g mL}^{-1}$ FK506-CO₂H solution containing 100×10^{-3} M EDC and 50×10^{-3} M NHS in MES buffer (0.05 M, pH 6.0) into each well. After at least 4 h of incubation, the wells were dumped and washed (3 \times 0.5 mL) with MES buffer. As a positive control, 60 $\mu\text{g mL}^{-1}$ D-biotin was used instead of FK506-CO₂H; the same protocol but in the absence of FK506-CO₂H was employed as negative control. In all cases, the functionalized wells were blocked with PBSS buffer for 1 h, rinsed with deionized water, dried under argon, and either used immediately or stored at 4 $^{\circ}\text{C}$.

Immunoassay Protocol: 150 μL of FK506 standard solution (in PBS) was mixed with 50 μL of antibody solution (anti-FK506 or anti-biotin antibody, 10 $\mu\text{g mL}^{-1}$ in PBS); then, the mixture was incubated in the FK506-coated well plates for 4 h. The wells were rinsed three times with 0.4 mL portions of PBSTM buffer, and 200 μL of a PBS solution containing 3 $\mu\text{g mL}^{-1}$ of fluoromagnetic nanoparticles functionalized with the detection antibody (see below) was added to each well and incubated for 3 h to reveal the surface-bound antibodies. A neodymium magnet used during the incubation step drives them to the bottom of the well, accelerating their binding to the IgM anti-Tacrolimus antibodies attached therein during the assay. The unbound nanoparticles were removed by rinsing with PBSTM (3 \times 0.4 mL) before the plate analysis.

Antibody Coupling to the Fluorescent Magnetic Nanoparticles: The detection antibodies (IgG anti IgM) were coupled to the carboxylated microspheres through the amine groups of the former using a carbodiimide-mediated procedure. According to the Estapor nanoparticles manufacturer, 50 μg of antibody are required to generate a monolayer of biomolecules on 1 mg of NPs. Unfortunately, nanoparticles are usually prone to aggregation due to their high surface area/volume ratio. Therefore, to avoid this problem and facilitate the complete coverage of their surface, a large excess of antibody (60 μg) was coupled to 0.2 mg of FMNPs using EDC/sulfo-NHS chemistry.

Supporting Information

Supporting Information is available from the Wiley Online Library or from the author.

Acknowledgements

This work was supported by the European Union NMP Research Program under contract no. 318372 ("NANODEM"), the Spanish Ministry of Economy and Competitiveness (Grant no. CTQ2015-69278-C2-R/AIE), and the European Funds for Regional Development (FEDER).

Conflict of Interest

The authors declare no conflict of interest.

Keywords

BODIPY, fluorescent magnetic nanoparticles, FRET, immunoassays, Tacrolimus

Received: November 1, 2017

Revised: January 30, 2018

Published online:

- [1] J. R. Lakowicz, *Principles of Fluorescence Spectroscopy*, 3rd ed., Springer, Berlin, Germany 2006.
- [2] a) L. Yuan, W. Lin, K. Zheng, L. He, W. Huang, *Chem. Soc. Rev.* **2013**, 42, 622; b) Z. Guo, S. Park, J. Yoon, I. Shin, *Chem. Soc. Rev.* **2014**, 43, 16.
- [3] a) S. Zhu, T. Fischer, W. Wan, A. B. Descalzo, K. Rurack, *Top. Curr. Chem.* **2011**, 300, 51; b) D. Genovese, E. Rampazzo, S. Bonacchi, M. Montalti, N. Zaccheroni, L. Prodi, *Nanoscale* **2014**, 6, 3022.
- [4] *The Immunoassay Handbook: Theory and Applications of Ligand Binding, ELISA and Related Techniques* (Ed: D. Wild), Elsevier, Amsterdam 2013.
- [5] a) J. M. W. van den Ouwelanda, I. P. Kema, *J. Chromatogr. B* **2012**, 883–884, 18; b) T. Cajka, O. Fiehn, *TrAC, Trends Anal. Chem.* **2014**, 61, 192; c) M. Karaźniewicz-Lada, A. Glowka, *J. Sep. Sci.* **2016**, 39, 132; d) A. Mika, P. Stepnowski, *J. Pharm. Biomed. Anal.* **2016**, 127, 207; e) K. Freudenberger, U. Hilbig, G. Gauglitz, *TrAC, Trends Anal. Chem.* **2016**, 79, 257.
- [6] a) T. Kino, H. Hatanaka, M. Hashimoto, M. Nishiyama, T. Goto, M. Okuhara, M. Kohsaka, H. Aoki, H. Imanaka, *J. Antibiot.* **1987**, XL, 1249; b) H. Tanaka, A. Kuroda, H. Marusawa, H. Hatanaka, T. Kino, T. Goto, M. Hashimoto, *J. Am. Chem. Soc.* **1987**, 109, 5031.
- [7] J. Clardy, *Proc. Natl. Acad. Sci. USA* **1995**, 92, 56.
- [8] a) D. H. Peters, A. Fitton, G. L. Plosker, D. Faulds, *Drugs* **1993**, 46, 746; b) N. A. Undre, P. Stevenson, A. Schafer, *Transpl. Proc.* **1999**, 31, 21; c) J. P. van Hoov, J. M. Boots, E. M. van Duijnhoven, M. H. Christiaans, *Transpl. Proc.* **1999**, 31, 54.
- [9] J. Schiff, E. Cole, M. Cantarovich, *Clin. J. Am. Soc. Nephrol.* **2007**, 2, 374.
- [10] *Point-of-Care Diagnostics on a Chip* (Eds: D. Issadore, R. M. Westervelt), Springer, Berlin, Germany 2013.
- [11] N. A. Stienstra, M. A. Sikma, A. L. van Dapperen, D. W. de Lange, E. M. van Maarseveen, *Ther. Drug Monit.* **2016**, 38, 722.
- [12] E. P. Córcoles, M. G. Boutelle, *Biosensors and Invasive Monitoring in Clinical Applications*, Springer, Berlin, Germany 2013.
- [13] J. Dietemann, P. Berthoux, J.-P. Gay-Montchamp, M. Batie, F. Berthoux, *Nephrol., Dial., Transplant.* **2001**, 16, 2246.
- [14] a) F. C. Grenier, J. Luczkiw, M. Bergmann, S. Lunetta, M. Morrison, D. Blonski, K. Shoemaker, M. Kobayashi, *Transplant. Proc.* **1991**, 23, 2748; b) J. L. Cogill, P. J. Taylor, I. S. Westley, R. G. Morris, S. V. Lynch, A. G. Johnson, *Clin. Chem.* **1998**, 44, 1942.

- [15] Y. Murakami, T. Endo, S. Yamamura, N. Nagatani, Y. Takamura, E. Tamiya, *Anal. Biochem.* **2004**, *334*, 111.
- [16] L. Rostaing, O. Cointault, P. Marquet, A.-G. Josse, M. Lavit, F. Saint-Marcoux, N. Kamar, *Transplant Int.* **2010**, *23*, 227.
- [17] K. Hirano, S. Maruyama, Y. Mino, T. Naito, J. Kawakami, *Clin. Biochem.* **2011**, *44*, 397.
- [18] a) *Standardization and Quality Assurance in Fluorescence Measurements I and II* (Eds: U. Resch-Genger, O. S. Wolfbeis), Springer Series on Fluorescence, Springer, Berlin, Germany **2008**; b) *Molecular Fluorescence Principles and Applications* (Ed: B. Valeur), Wiley VCH, Weinheim, Germany **2002**.
- [19] For some general reviews see: a) G. Ulrich, R. Ziessel, A. Harriman, *Angew. Chem.* **2008**, *120*, 1202; *Angew. Chem., Int. Ed.* **2008**, *47*, 1184; b) A. Loudet, K. Burgess, *Chem. Rev.* **2007**, *107*, 4891; c) N. Boens, B. Verbelen, W. Dehaen, *Eur. J. Org. Chem.* **2015**, **2015**, 6577.
- [20] a) K. Rurack, M. Kollmannsberger, J. Daub, *New J. Chem.* **2001**, *25*, 289; b) Y.-H. Yu, A. B. Descalzo, Z. Shen, H. Röhr, Q. Liu, Y.-W. Wang, M. Spieles, Y.-Z. Li, K. Rurack, X.-Z. You, *Chem.-Asian J.* **2006**, *1*, 176; c) K. Umezawa, Y. Nakamura, H. Makino, D. Citterio, K. Suzuki, *J. Am. Chem. Soc.* **2008**, *130*, 1550; d) Y. Hayashi, N. Obata, M. Tamaru, S. Yamaguchi, Y. Matsuo, A. Saeki, S. Seki, Y. Kureishi, S. Saito, S. Yamaguchi, H. Shinokubo, *Org. Lett.* **2012**, *14*, 866; e) Y. Ni, W. Zeng, K.-W. Huang, J. Wu, *Chem. Commun.* **2013**, *49*, 1217; f) M. Hecht, T. Fischer, P. Diedrich, W. Kraus, A. B. Descalzo, W. E. S. Unger, K. Rurack, *Chem. Open* **2013**, *2*, 25; g) Y. Ni, J. Wu, *Org. Biomol. Chem.* **2014**, *12*, 3774.
- [21] a) L. Wang, W. Tan, *Nano Lett.* **2006**, *6*, 84; b) J. Xu, J. Liang, J. Li, W. Yang, *Langmuir* **2010**, *26*, 15722; c) J. Yu, X. Diao, X. Zhang, X. Chen, X. Hao, W. Li, X. Zhang, C.-S. Lee, *Small* **2014**, *10*, 1125.
- [22] a) A. B. Descalzo, H.-J. Xu, Z.-L. Xue, K. Hoffmann, Z. Shen, M. G. Weller, X.-Z. You, K. Rurack, *Org. Lett.* **2008**, *10*, 1581; b) T. Behnke, C. Würth, K. Hoffmann, M. Hübner, U. Panne, U. Resch-Genger, *J. Fluoresc.* **2011**, *21*, 937.
- [23] M. A. H. Alamiry, A. C. Benniston, J. Hagon, T. P. L. Winstanley, H. Lemmetyinen, N. V. Tkachenko, *RSC Adv.* **2012**, *2*, 4944.
- [24] a) G. Vives, G. Giansante, R. Bofinger, G. Raffy, A. del Guerso, B. Kauffmann, P. Batat, G. Jonusauskas, N. D. McClenaghan, *Chem. Commun.* **2011**, *47*, 10425; b) O. Galangau, C. Dumas-Verdes, R. Méallet-Renault, G. Clavier, *Org. Biomol. Chem.* **2010**, *8*, 4546.
- [25] a) S. E. Braslavsky, *IUPAC* **2007**, *79*, 293; b) *FRET – Förster Resonance Energy Transfer: From Theory to Applications* (Eds: I. Medintz, J.N. Hildebrandt), Wiley-VCH, Weinheim, Germany **2014**.
- [26] *Handbook of Chemistry and Physics*, 89th ed. (Ed: D. R. Lide), CRC Press, Boca Raton, FL, USA **2009**.
- [27] P. Wu, L. Brand, *Anal. Biochem.* **1994**, *218*, 1.
- [28] M. J. Mayoral, P. Ovejero, M. Cano, G. Orellana, *Dalton Trans.* **2011**, *40*, 377.
- [29] E. R. Carraway, J. N. Demas, B. A. DeGraff, *Anal. Chem.* **1991**, *63*, 332.
- [30] J. N. Demas, *Excited State Lifetime Measurements*, Academic Press, New York **1983**.
- [31] G. Orellana, in *Optical Chemical Sensors* (Eds: F. Baldini, A. N. Chester, J. Homola, S. Martellucci), NATO Sci. Ser. II, vol. 224, Springer, Berlin, Germany **2006**, pp. 99–116.
- [32] C.-J. Yu, S.-M. Wu, W.-L. Tseng, *Anal. Chem.* **2013**, *85*, 8559.
- [33] D. M. Rissin, C. W. Kan, T. G. Campbell, S. C. Howes, D. R. Fournier, L. Song, T. Piech, P. P. Patel, L. Chang, A. J. Rivnak, E. P. Ferrell, J. D. Randall, G. K. Provuncher, D. R. Walt, D. C. Duffy, *Nat. Biotechnol.* **2010**, *28*, 595.
- [34] W. Kusnezow, J. D. Hoheisel, *J. Mol. Recognit.* **2003**, *16*, 165.
- [35] R. F. Masseyeff, W. H. Albert, N. A. Staines, *Methods of Immunological Analysis*, 1st ed., Wiley-VCH, New York **1992**, pp. 655–671.
- [36] P. Wallemacq, V. W. Armstrong, M. Brunet, V. Haufroid, D. W. Holt, A. Johnston, D. Kuypers, Y. Le Meur, P. Marquet, M. Oellerich, E. Thervet, B. Toenshoff, N. Undre, L. T. Weber, I. S. Westley, M. Mourad, *Ther. Drug Monit.* **2009**, *31*, 139.
- [37] M. Menotta, S. Biagiotti, L. Streppa, L. Rossi, M. Magnani, *Anal. Chim. Acta* **2015**, *884*, 90.
- [38] C. Berrettoni, S. Berneschi, R. Bernini, A. Giannetti, I. A. Grimaldi, G. Persichetti, G. Testa, S. Tombelli, C. Trono, F. Baldini, *Procedia Eng.* **2014**, *87*, 392.
- [39] C.-M. Cheng, C.-M. Kuan, C.-F. Chen, *In-Vitro Diagnostic Devices: Introduction to Current Point-of-Care Diagnostic Devices*, Springer, Berlin, Germany **2016**.
- [40] O. Cañadas, A. Sáenz, G. Orellana, C. Casals, *Anal. Biochem.* **2005**, *340*, 57.
- [41] R. F. Kubin, A. N. Fletcher, *J. Lumin.* **1982**, *27*, 455.
- [42] K. Rurack, M. Spieles, *Anal. Chem.* **2011**, *83*, 1232.